

# Molecular Origin of the Self-Assembled Morphological Difference Caused by Varying the Order of Charged Residues in Short Peptides

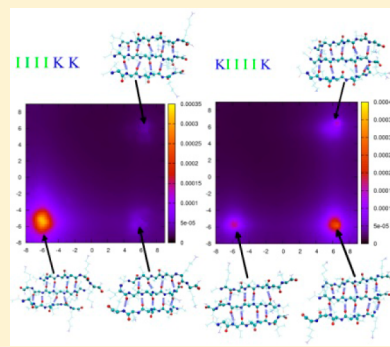
Li Deng,<sup>†</sup> Peng Zhou,<sup>†</sup> Yurong Zhao,<sup>†</sup> Yanting Wang<sup>\*,‡</sup> and Hai Xu<sup>\*,†</sup>

<sup>†</sup>Centre for Bioengineering and Biotechnology, China University of Petroleum (East China), 66 Changjiang West Road, Qingdao 266580, China

<sup>‡</sup>State Key Laboratory of Theoretical Physics, Institute of Theoretical Physics, Chinese Academy of Sciences, 55 East Zhongguancun Road, P.O. Box 2735, Beijing 100190, China

## Supporting Information

**ABSTRACT:** In order to understand how microscopic molecular interactions between short peptides determine their mesoscopic self-assembled morphology, we studied the microscopic assembled structures of the short peptides I4K2 and KI4K, which have the same amino acid composition but different sequences, by using all-atom replica exchange molecular dynamics simulation. We found that, at room temperature, the difference in amino acid sequence does not apparently alter their strong propensity of forming  $\beta$ -sheets but does strongly affect their assembled stable structures and their appearance probabilities. These differences result from the competition between the electrostatic and hydrophobic interactions among the side chains of the molecules, which are linked up by hydrogen bonds formed between neighboring peptide backbones. Our simulation results not only reveal the molecular origin of the self-assembled morphological difference between I4K2 and KI4K but also demonstrate in general the subtle balance between electrostatic, hydrophobic, and hydrogen bonding interactions in short-peptide self-assembly.



## I. INTRODUCTION

The self-assembly of peptides has been intensively studied in various kinds of systems, such as chemical materials, nanotechnology, and biological medicines.<sup>1–3</sup> Peptide self-assemblies have shown well-defined nanostructures and unique properties and functions, thus having great potential in a variety of applications in the fields of material science, nanotechnology, and biotechnology.<sup>4,5</sup> On the other hand, the fibrillar structures self-assembled by  $A\beta$  peptides are regarded as the putative causative agent in amyloid diseases and are thus of great importance. These nanostructures have been widely observed in both experimental and simulation studies of Alzheimer's disease<sup>6,7</sup> and other neurodegenerative diseases.<sup>8,9</sup> Various experimental methods, such as circular dichroism spectroscopy, fiber XRD, and NMR,<sup>10–12</sup> have shown that the fibrils are composed of regular secondary structures, such as  $\beta$ -sheet. To develop novel functions and applications based on peptide assembly and combat against neurodegenerative diseases, it is imperative to thoroughly understand the rationales and rules that govern peptide assembly.

Because of the low cost of their synthesis, the ease of engineering their primary sequences and tuning their molecular properties, and their structural stability, more and more short peptides (typically less than 10 residues) have been explored in recent years, in particular for research aiming at the establishment of the relationship between peptide primary sequences and assembled nanostructures and properties and the rational interpretation of the involved noncovalent forces

during peptide self-assembly.<sup>13–20</sup> Typical short self-assembling peptides include fragments of  $A\beta$  peptides and their derivatives and designed amphiphilic peptides. For instance, KLVFFAE ( $A\beta(16–22)$ ) and even the more short derivative KFFE have been found to form amyloid-like fibrils in an appropriate pH solution with antiparallel  $\beta$ -sheet structures.<sup>21,22</sup> The molecular features of both KFFE and KLVFFAE include a hydrophobic core within the sequence and oppositely charged side chains at the N-terminal and C-terminal, with the ionic complementarity being responsible for the formation of antiparallel  $\beta$ -sheet structuring. For another instance, ImK ( $m = 3–5$ ) peptides designed by us can readily self-assemble into long and stable nanofibrils in aqueous solutions, driven by the combination of hydrogen bonds between peptide backbones, hydrophobic interactions between hydrophobic side chains, and electrostatic interaction between charged side chains. In a very recent experimental study, we have designed two short peptides IIIIKK (I4K2) and KIIIIK (KI4K), which only differ from the positions of the charged amino acid residues.<sup>23</sup> Under exactly the same experimental condition, the two peptides self-assembled to form totally different mesoscopic morphologies: I4K2 formed twisted ribbons with 10–15 nm width, while KI4K formed nanotubes with 80–100 nm width (Figure S1). This demonstrates that the charged side chains of amino acid

Received: June 26, 2014

Revised: September 25, 2014

Published: October 8, 2014



residues strongly affect the self-assembled morphologies of short peptides as well as the self-assembly processes.

Despite the simple molecular structures of short peptides, their energy landscapes are still complex upon self-assembly, therefore allowing them to be ideal systems for understanding the role of competitive molecular interactions.<sup>24</sup> Many theoretical studies have thus been devoted to model the key steps in the self-assembly processes of short peptides and to mechanistically explain the morphological transitions tuned by changing physical chemistry conditions or molecular structures of peptides. Aggeli et al.<sup>13,25,26</sup> have proposed a hierarchical model that decomposes the self-assembly process into several subprocesses with different time scales and driving forces. According to this hierarchical model, the competition between the attractive energy among tapes (long  $\beta$ -sheet structures) and the elastic energy cost of tape deformation determines the width of the self-assembled structure. Some elastic theories<sup>27–30</sup> were developed and reached the same conclusion that the width of the self-assembled structure has a direct relation with the morphology self-assembled by peptide: when the width is larger than a critical value, the helical structure has a lower elastic energy than the twisted structure, and vice versa. This conclusion is consistent with recent experimental results conducted by Childers et al.<sup>31</sup> and also applicable to our study<sup>23</sup> in which the width of the twisted ribbons self-assembled by I4K2 is obviously smaller than the width of the nanotubes self-assembled by KI4K.

In spite of the large number of experimental and theoretical studies conducted on peptide self-assembly that provided some insights into the mechanistic understanding of peptide self-assembly, it is still unclear how the microscopic molecular details affect the mesoscopic self-assembled morphology and self-assembly process. To bridge the gap between theories and experiments, some researchers have conducted computer simulations on peptide self-assembly.<sup>32–37</sup> Because the regular molecular dynamics (MD) simulation methods are generally inadequate in sampling the energy landscapes of many peptides system, accelerated algorithms, such as the umbrella sampling method<sup>38,39</sup> and the replica exchange molecular dynamics (REMD) method,<sup>40,41</sup> are employed to simulate the peptide self-assembly. The umbrella sampling method enhances the sampling of high-energy configurations by restricting the system to evolve in a certain range along a special reaction coordinate, and it has been used to study the microscopic driving force in peptide self-assembly processes.<sup>42,43</sup> In an REMD, many replicas of the MD (or Monte Carlo) simulations of the same system at different temperatures are conducted simultaneously, and the configurations in different replicas are allowed to exchange with a certain probability. In this way, the REMD can significantly accelerate the sampling of energy landscapes at low temperatures. The energy landscape of a KLVFFAE dimer was studied by all-atom REMD,<sup>44</sup> which indicated that the aggregated dimers of this peptide adopt not only parallel or antiparallel conformations observed in amyloid fibrils but also some cross-conformations with strands perpendicular to each other. By conducting a series of all-atom REMD simulations for a KFFE dimer,<sup>45</sup> it was found that the opposite charges in the two end groups play an important role in stabilizing the structure of the KFFE oligomers.

Our experimental study of the I4K2 and KI4K peptides<sup>23</sup> indicated that these two peptides are good and simple model systems for studying the charge effect on peptide self-assembly. In this work, we use all-atom REMD simulations to explore the

conformations of an I4K2 trimer and a KI4K trimer in an explicit solvent. Our results have shown that both I4K2 and KI4K have a strong propensity to form  $\beta$ -sheet structures, but with apparent structural differences. The analysis of the short-range interaction has demonstrated that the hydrogen-bonding interactions between the two backbones of the neighboring peptides are the main driving force to form  $\beta$ -sheet structures. Detailed analysis of the stable structures of the I4K2 and KI4K trimers demonstrate that the I4K2 monomers have a weaker propensity than KI4K to have the laminated growth by layer-layer stacking, consistent with previous theoretical<sup>26</sup> and experimental<sup>23</sup> results. A general conclusion drawn from this study is that the positions of charged residues in an amino acid sequence have a strong influence on the earlier steps of oligomer structure formation, which leads to different mesoscopic self-assembled morphologies.

## II. METHODS

**2.1. Simulation Methods.** In this work, we have done regular MD simulations for a peptide monomer and REMD simulations for a peptide trimer for both I4K2 and KI4K in solvent, respectively, by using the GROMACS software package.<sup>46</sup> In those two kinds of all-atom simulations, the OPLS-AA force field<sup>47</sup> was used to model the two short peptides and the TIP4P model<sup>48</sup> was used to model water molecules. In all simulations, the electrostatic interactions were treated with the particle-mesh-Ewald method,<sup>49,50</sup> and both the cutoff of the van der Waals (VDW) interactions and the cutoff of the electrostatic interactions in real space were set to be 1.2 nm. In the I4K2 monomer simulation, the cubic box has a side length of 4.996 nm and contains 4078 water molecules and 2 Cl<sup>−</sup> counterions. In the KI4K monomer simulation, the cubic box has a side length of 4.998 nm and contains 4079 water molecules and 2 Cl<sup>−</sup> counterions. Each monomer simulation was conducted in a constant NPT ensemble at a pressure  $P = 1$  atm and a temperature  $T = 300$  K for 20 ns with 400 configurations evenly sampled from the trajectory. The system temperature was kept constant by a Nosé–Hoover thermostat<sup>51,52</sup> with a coupling time of 0.1 ps, and the system pressure was kept constant by a Parrinello–Rahman barostat<sup>53,54</sup> with a coupling time of 0.5 ps.

In the REMD simulations for I4K2, the three monomers were put in a cubic simulation box with a side length of 3.39 nm, together with 1184 water molecules and 6 Cl<sup>−</sup> counterions. In the KI4K REMD simulation, the cubic simulation box has a side length of 3.40 nm containing 1179 water molecules and 6 Cl<sup>−</sup> counterions. The initial configuration of a REMD simulation was randomly chosen from the trajectory of a regular NVT MD simulation for the trimer at  $T = 1000$  K. The REMD simulations were conducted in a constant NVT ensemble for 240 ns with 6000 configurations evenly sampled from the trajectory. The temperature was kept constant by a Nosé–Hoover thermostat<sup>51,52</sup> with a coupling time of 0.1 ps. For both peptides, we simultaneously simulated 38 replicas with the temperatures ranging from 300 to 600 K. The temperatures were so chosen to ensure that the exchange rates among replicas remained in the range from 18% to 34%. The configuration exchanges were attempted every 1000 steps (2 ps). In all simulations, the integration time step was 2 fs and the periodic boundary condition was applied to all three dimensions.

**2.2. Labeling Method for a Trimer.** In the REMD simulations, the monomers in a trimer frequently switch their

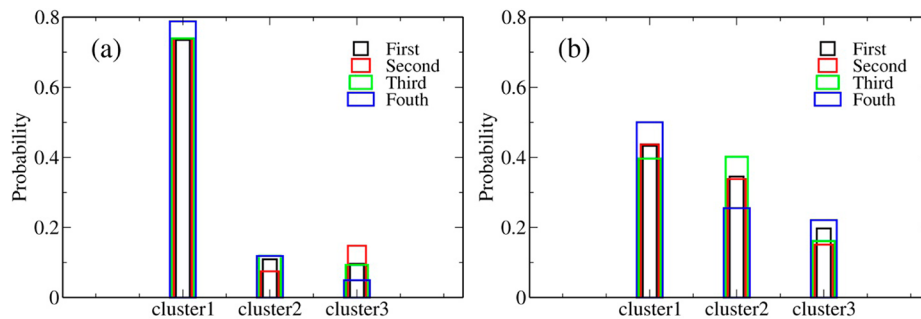


**Figure 1.** Cluster appearance histograms of the configurations sampled in the four successive 40 ns REMD simulations at  $T = 300$  K for I4K2 (a) and KI4K (b).

relative positions. Consequently, if we simply label the monomers by their initial positions, two trimers with the same structure will be frequently identified as totally different structures due to the reordering of monomer positions. To avoid this problem, for each sampled configuration, we relabeled the three monomers in a trimer with the following rules. First, the monomer having the shortest total distance to the other two monomers is identified as the middle one and labeled as monomer 2 (M2). Then the relative orientations of the other two monomers are checked: if they are parallel, monomer 1 (M1) is the one which is closer to M2 and the other one is labeled as monomer 3 (M3); if they are antiparallel, M1 is the one parallel to M2 and the other is labeled as M3.

**2.3. Clustering and Analyzing Methods.** To identify stable trimer structures, the sampled trimer configurations need to be grouped into several clusters according to the structural similarities of the configurations. The Daura cluster analysis method<sup>55</sup> was used to group the configurations sampled from the REMD simulation trajectories as follows. First, the  $C_\alpha$  root-mean-square deviation (RMSD) is calculated for all pairs of sampled configurations, and if the RMSD is less than 0.25 nm, the two configurations are regarded as “neighbors”. Second, the configuration with the largest number of neighbors is identified as the central structure, and the largest cluster is composed of this central configuration and its neighbors. Third, the configurations in the largest cluster are eliminated from the set of sampled configurations. Finally, the above processes are repeated until no sampled configurations left. For all the configurations, the DSSP program<sup>56</sup> was used to assign a secondary structure to each residue in the peptide. To quantify the difference between the  $\beta$ -sheet structures formed by I4K2 and KI4K, we calculated the end-to-end distance of the backbone, the RMSD of any two peptides, the tilt angle, the twist angle, the contact degree, and the number of hydrogen bonds between two neighboring peptides. The trimer energy landscape in a solvent can then be constructed with a combination of these quantities. The end-to-end distance of a peptide  $i$  is defined as the distance between the  $C_\alpha$  atom in the N-terminal residue  $\vec{r}_i^N$  ( $C_\alpha$ ) and the  $C_\alpha$  in the C-terminal residue  $\vec{r}_i^C$  ( $C_\alpha$ ):

$$d_i = |\vec{d}_i| = |\vec{r}_i^N(C_\alpha) - \vec{r}_i^C(C_\alpha)| \quad (1)$$

The tilt angle  $\theta_{ij}$  between the backbones of two neighboring peptides  $i$  and  $j$  is defined as

$$\cos(\theta_{ij}) = \frac{\vec{d}_i \cdot \vec{d}_j}{|\vec{d}_i| \cdot |\vec{d}_j|} \quad (2)$$

The tilt angle  $\theta_{ij}$  was used to determine whether the two peptides are parallel or antiparallel: the two peptides are parallel if  $\theta_{ij}$  is smaller than  $\pi/2$ , and vice versa. The twist angle  $\gamma_{ij}$  between two neighboring peptides is directly related to the tilt angle  $\theta_{ij}$  by

$$\gamma_{ij} = \begin{cases} \theta_{ij} & \text{if } \theta_{ij} < \frac{\pi}{2} \\ \pi - \theta_{ij} & \text{else} \end{cases} \quad (3)$$

The contact degree between a pair of  $C_\alpha$  atoms belonging to two different peptides is defined as

$$g_{ij}^{mn} = \begin{cases} 1 - r_{ij}^{mn} & \text{if } r_{ij}^{mn} < 0.65 \text{ nm} \\ 0 & \text{else} \end{cases} \quad (4)$$

where  $r_{ij}^{mn}$  is the distance between  $C_\alpha$  atom  $m$  in peptide  $i$  and  $C_\alpha$  atom  $n$  in peptide  $j$ . The contact degree  $g_{ij}$  for two neighboring peptides  $i$  and  $j$  is then defined as the sum of the contact degrees of all  $C_\alpha$  atom pairs between the two peptides:

$$g_{ij} = (-1)^s \sum_{m,n} g_{ij}^{mn}, \quad s = \begin{cases} 0 & \text{if } i \text{ and } j \text{ are parallel} \\ 1 & \text{else} \end{cases} \quad (5)$$

In order to understand the physical driving forces for peptide self-assembly, the nonbonded energies, including the van der Waals (VDW) and electrostatic interactions, between two neighboring peptides were recalculated for all the configurations sampled from the REMD trajectories. The calculations of the nonbonded energies were limited to those atom pairs whose interatomic distances are less than 1.2 nm.

### III. RESULTS AND DISCUSSION

**3.1. Trimer Structures.** Since our previous experimental study on I4K2 and KI4K was performed at room temperature,<sup>23</sup> we concentrate on analyzing our REMD simulation results at  $T = 300$  K. To verify that the REMD simulations sample adequately the simulated trimer systems for both peptides, we plot the cluster appearance histograms of the trimer structures sampled from four successive 40 ns simulations at  $T = 300$  K in Figure 1. Figure 1a shows the results for I4K2, and Figure 1b is for KI4K. In those figures, “cluster 1”, “cluster 2”, and “cluster 3” are the three largest clusters determined by the clustering method. The histograms demonstrate that the sampling is adequate, since the four

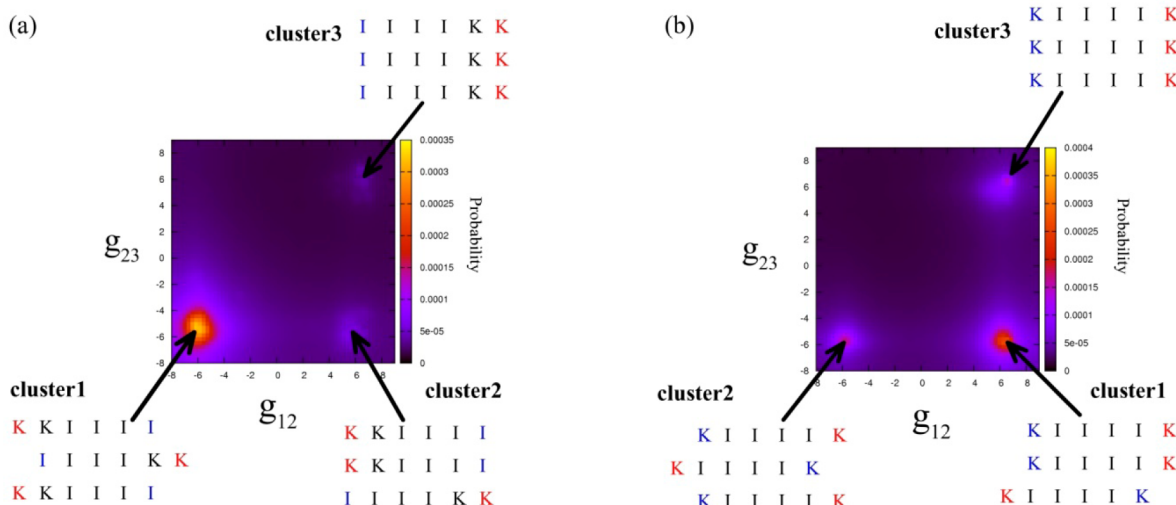


**Figure 2.** Probability maps of structures sampled in the REMD simulations and symbolic representations of three typical structures for I4K2 (a) and KI4K (b) at  $T = 300$  K. Each structure is characterized by the contact degree between M1 and M2 and between M2 and M3 in the probability map. In the symbolic representations, residues marked blue are at the N-terminal and those marked red are at the C-terminal.

independent simulations provide similar configurational distributions.

As shown in Figure 1, both I4K2 and KI4K have about 95% sampled configurations belonging to the three most probable clusters whose structures are all  $\beta$ -sheets, as discussed below, indicating that I4K2 and KI4K have a strong propensity to form  $\beta$ -sheet structures at  $T = 300$  K. On the other hand, the probability distributions for the two peptide systems are very different, indicating that changing the amino acid sequence has significant influences on the stable microscopic structures.

The probability maps of the trimer structures at  $T = 300$  K for I4K2 and KI4K are shown in Figures 2a and 2b, respectively. The X-axis is the contact degree  $g_{12}$  between M1 and M2, and the Y-axis is the contact degree  $g_{23}$  between M2 and M3. The amino acid sequences of the three typical  $\beta$ -sheet structures are symbolically represented around the probability maps, and the corresponding trimer conformations are shown in Figure 3. It can be seen from Figure 3 that there exist many hydrogen bonds between the backbones of two neighboring peptides, which enables the trimers to form  $\beta$ -sheet structures. In addition, the probability maps demonstrate that all trimer structures sampled from the REMD simulations at  $T = 300$  K have a large contact degree between neighboring peptides, which means that both peptides have a strong propensity to aggregate at room temperature. The structures shown in Figure 3 indicate that the aggregates formed by both peptides have a  $\beta$ -sheet structure, consistent with the experimental results.<sup>23</sup> Nevertheless, the structures formed by different peptides have obvious differences.

The differences between I4K2 and KI4K structures in Figures 1–3 are analyzed as follows. For I4K2, cluster 1 has an appearance probability of 75.0%, cluster 2 is 10.5%, cluster 3 is 9.6%, and only a very small portion of the sampled configurations does not belong to the three clusters. In cluster 1, both M1 and M3 are antiparallel to M2 with one amino acid residue shift, leading to the more significant exposure of the charged residues in all three C-terminals to the solvent. In cluster 2, M1 is parallel to M2 and antiparallel to M3 without position shift. In cluster 3, both M1 and M3 are parallel to M2 without position shift. For KI4K, cluster 1 has a probability of

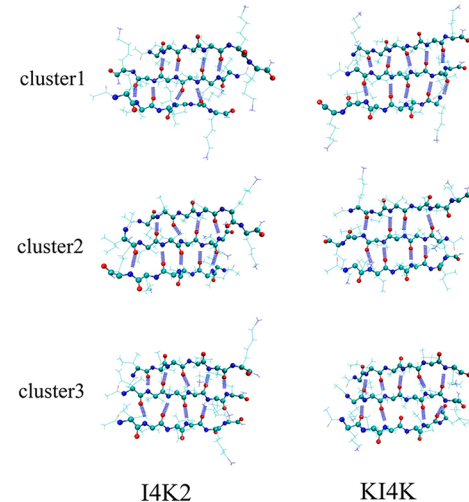


**Figure 3.** Top three most probable conformations of I4K2 and KI4K trimers. The hydrogen bonds between neighboring backbones are illustrated by wide dotted lines. Carbon atoms are colored cyan, nitrogen blue, and oxygen red.

44.1%, cluster 2 is 33.5%, cluster 3 is 18.2%, and the appearance of other structures is rare. In cluster 1, M1 is parallel to M2 without position shift, and M3 is antiparallel to M2 with one residue shift. In cluster 2, both M1 and M3 are antiparallel to M2 with one residue shift, leading to more significant exposure of the charged residues than that in the structure with no shift due to the steric hindrance. In cluster 3, both M1 and M3 are parallel to M2 without position shift.

The physical origin of the above structural differences can be attributed to different charge distributions in I4K2 and KI4K molecules because both peptides have the same hydrophobic core which is composed of four isoleucines. For I4K2, since the two charged K residues are both on the C-terminal, the antiparallel alignment of neighboring peptides lowers the electrostatic interaction by avoiding the close contact of the same-charged residues, and one shift alignment with the C-terminals significantly exposed in water maximizes the system entropy by increasing the hydrophilic surface between charged

residues and water molecules. Both factors enable an antiparallel  $\beta$ -sheet to have a lower free energy than a parallel  $\beta$ -sheet in the self-assembly, so cluster 1 with two antiparallel structures has the lowest free energy and highest appearance probability; cluster 3 with two parallel structures has the highest free energy and the lowest appearance probability; and cluster 2 with mixed structures has an intermediate appearance probability. Nevertheless, the effect of electrostatic and hydrophobic interactions is not strong enough to exclude the appearance of other two typical structures that violate the above arrangements. In contrast, for KI4K, one K residue is on the N-terminal and the other is on the C-terminal, so the antiparallel and parallel  $\beta$ -sheet structures have similar electrostatic interactions and their free energy difference is small. Consequently, cluster 2 with two antiparallel  $\beta$ -sheets only has a little larger appearance probability than cluster 3 with two parallel  $\beta$ -sheets, and cluster 1 with a mixture of two structures has the largest appearance probability because it combines both antiparallel and parallel structures. In addition, the potential of mean force (PMF) is calculated for both peptides with the reaction coordinate of the center-of-mass distance (shown in Figure S2) between two neighboring molecules. As shown in Figure S3 of the Supporting Information, the I4K2 PMF is very different from KI4K, consistent with the parallel and antiparallel conformational difference between neighboring molecules in I4K2 and KI4K.

The results of the REMD simulations at higher temperatures provide further information about the thermal stabilities of different trimer structures. The appearance probabilities of three typical structures and total cluster number versus temperature are shown in Figure 4. Both peptides have similar trends of appearance probability changes with temperature: when the temperature is low, the total appearance probability of the three typical structures is almost one; with increasing temperature, the appearance probabilities of cluster 1 and cluster 3 decrease monotonically, but the appearance probability of cluster 2 slightly increases before decreasing. When the system is at high temperatures, the total cluster number rapidly increases and the total appearance probabilities of the three typical structures significantly decrease with increasing temperature because larger thermal fluctuation breaks more hydrogen bonds and thus results in more disordered structures. KI4K is thermally more stable than I4K2 since KI4K always has fewer structures appear at the same temperature.

**3.2. Molecular Origin of the  $\beta$ -Sheet Formation.** From the REMD results, we can see that both I4K2 and KI4K have a strong propensity to form  $\beta$ -sheet structures at room temperature. To discover its molecular origin, we calculated the total number of hydrogen bonds and the number of residues belonging to the  $\beta$ -sheet structures of trimers, as shown in Figure 5.

Since there are seven hydrogen bond acceptors and donors on a backbone, the maximum number of available hydrogen bonds in a trimer is 14. In Figure 5, we can observe an apparent correlation between the total number of hydrogen bonds and the number of residues belonging to the  $\beta$ -sheet structures. For I4K2, the average number of hydrogen bonds and residues are  $9.8 \pm 1.3$  and  $10.4 \pm 1.2$ , respectively. For KI4K, those values are  $10.5 \pm 1.1$  and  $10.2 \pm 1.2$ . Since the average number of residues is similar to the number of hydrogen bonds, it can be concluded that the hydrogen bonds formed between the

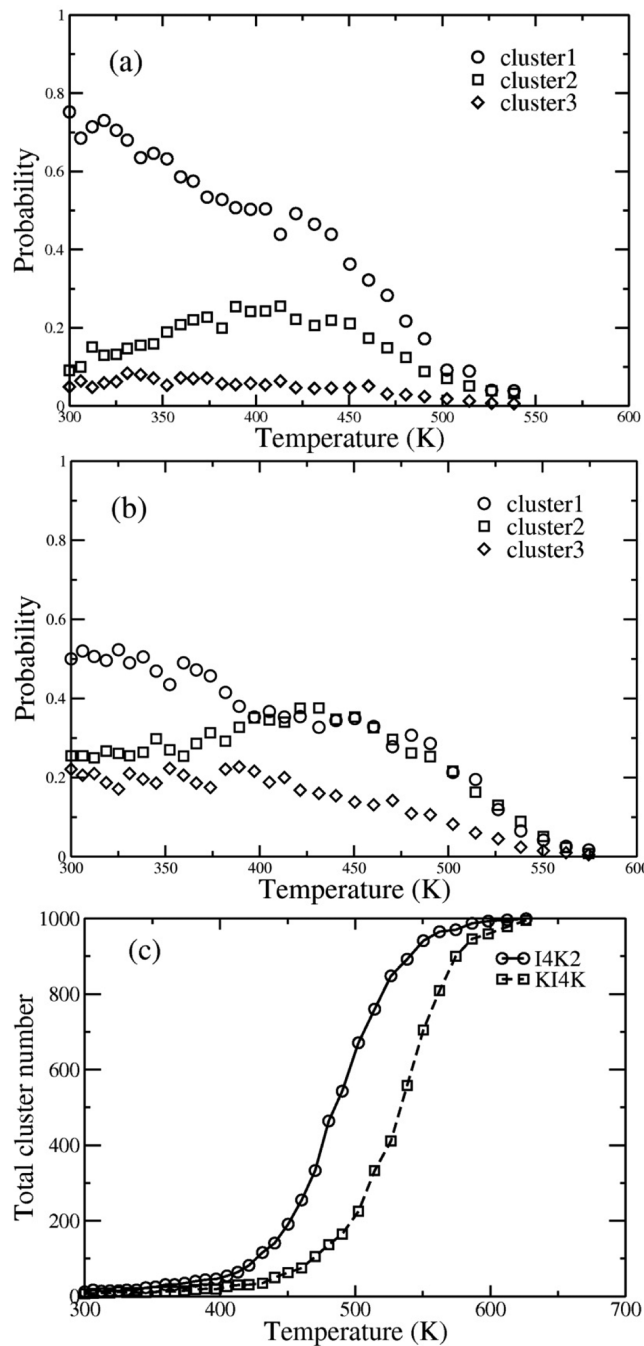


**Figure 4.** Appearance probabilities of the top three clusters versus temperature for I4K2 (a) and KI4K (b) and the total cluster number versus temperature for both I4K2 and KI4K (c).

backbones play the major role in thermally stabilizing the  $\beta$ -sheet structures.

Energy analysis provides more physical insights into the formation of the trimer structures. The short-range energies, which are the sum of the total VDW and Coulomb interactions over all pairs of nonbonded atoms within a distance smaller than 1.2 nm, were calculated for all sampled configurations. The average short-range energy of I4K2 in the monomer MD simulation is  $626 \pm 20$  kJ/mol, and that of KI4K is  $590 \pm 18$  kJ/mol. In contrast, the average short-range energy for a single I4K2 molecule in the trimer by REMD simulation is  $631 \pm 17$  kJ/mol and that for KI4K is  $624 \pm 16$  kJ/mol, close to the

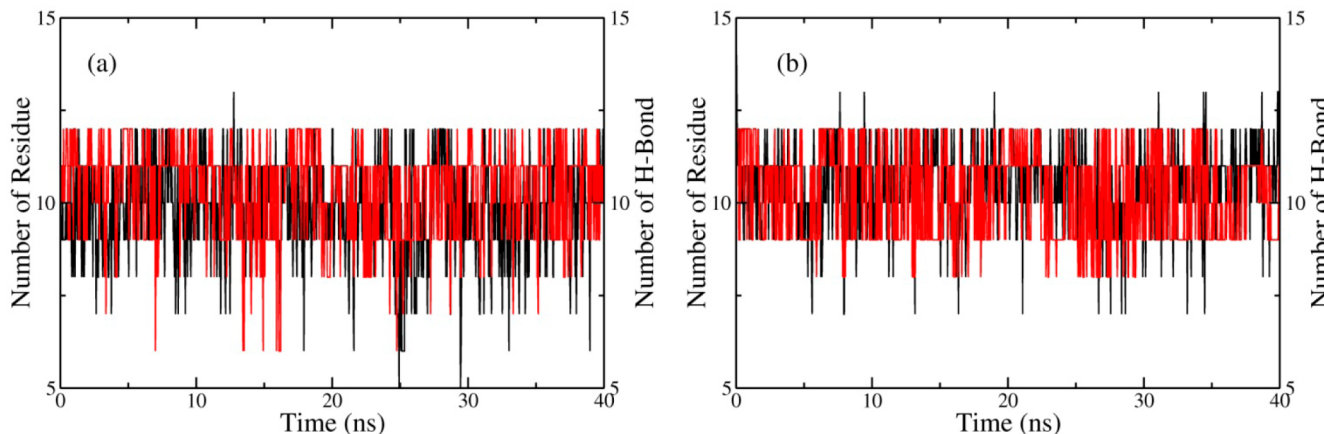


**Figure 5.** Number of hydrogen bonds (black lines) and number of residues (red lines) belonging to the  $\beta$ -sheet structure for I4K2 (a) and KI4K (b) trimers at  $T = 300$  K.

values from the monomer MD simulations, indicating that different residue sequences and interactions between peptides do not obviously affect the short-range energy of monomer. On the other hand, the average short-range energy between two neighboring peptides of the I4K2 trimer is  $-249 \pm 28$  and  $-250 \pm 27$  kJ/mol for KI4K. The negative values of these intermolecular short-range interactions indicate that the VDW and Coulomb nonbonded interactions between two neighboring peptides are attractive driving forces for  $\beta$ -sheet formation.

The average numbers of hydrogen bonds and residues in  $\beta$ -sheet structure at different temperatures are shown in Figure 6a, and the short-range energies between two neighboring peptides at different temperatures are shown in Figure 6b. The average number of residues in  $\beta$ -sheet structure is close to the average number of hydrogen bonds at all temperatures, consistent with the results at  $T = 300$  K. The average number of hydrogen bonds decreases with increasing temperature, but the average short-range energy increases with temperature. Below a certain temperature, the number of hydrogen bonds and the short-range energy change slowly, and they change rapidly above the temperature. These results indicate that the short-range energy between neighboring peptides determines the stability of the  $\beta$ -sheet structure and the  $\beta$ -sheet trimer dissociates at high temperatures when the thermal fluctuation overrides the attractive short-range energy. The intermolecular short-range energy versus the number of hydrogen bonds in a trimer at all temperatures is shown in Figure 6c. It is apparent that they have a nearly linear relation. Linear fitting of the curves determines that the correlation between the interaction between neighboring peptides and the number of hydrogen bonds are larger than 0.9 for both peptides, indicating that the nonbonded interactions between neighboring peptides is the physical driving force to form hydrogen bonds between peptide backbones and to thermally stabilize the trimers with the  $\beta$ -sheet structure.

**3.3. Initial Microscopic Structure in the Self-Assembled Morphology Formation.** Our experiments have demonstrated that, under the same physical condition, I4K2 can self-assemble to form twisted ribbons with the widths of 10–15 nm, while KI4K can self-assemble to form nanotubes with the diameters of 80–160 nm (Figure S1). Both morphologies have a thickness of a single molecule. On the other hand, as discussed before, our REMD simulation results show that the energy landscapes of I4K2 and KI4K are

significantly different. The hierarchical model proposed by Aggeli et al.<sup>13,25,26</sup> regards the peptide molecule as a rigid rod and assumes that the peptide growth is along the hydrogen-bond direction, and the tape growth along the side-chain direction is driven by the hydrophobic interaction between the hydrophobic side chains. Under the framework of Aggeli's model, we now discuss how the simulated microscopic structural differences of the two peptides lead to their different mesoscopic self-assembled structures.

In Figure 7, the end-to-end distances of the molecules in the  $\beta$ -sheet structure are shown in (a) and (b) for I4K2 and KI4K, respectively. For I4K2 and KI4K trimers, since M2 can form hydrogen bonds with both M1 and M3, M2 is more extended than M1 and M3. The M1 and M3 in KI4K have similar end-to-end distances, but M1 and M3 in I4K2 are quite different due to the asymmetry of molecular charge distributions. The average end-to-end distances in the  $\beta$ -sheet structure simulated by REMD are shown in (c), and the end-to-end distances for a free monomer in solvent simulated by regular MD are shown in (d). Comparing the results for the free monomer and the trimer, it is clear that the molecules in the  $\beta$ -sheet structures are more extended than the free monomers in solvent because the hydrogen bonds formed between the peptide backbones extend the molecules, but the hydrogen bonds between the peptide backbones and water molecules do not. Because of the asymmetric charge distribution, the peak value of the end-to-end distance of the I4K2 monomer in water is 1.5 nm, much smaller than the average value in trimer (1.9 nm), demonstrating that the peptides do not have to be rodlike in the self-assembly process as assumed by Aggeli's hierarchical model and the interaction between peptide have strong effect on the conformation of peptide.

To understand how the monomer distortion affects the initial self-assembly process, the RMSD distributions between the monomer configurations sampled in the REMD simulations and a fully extended reference monomer structure have been calculated and are shown in Figure 8a. The peak position for I4K2 is around 0.22 and 0.15 nm for KI4K, indicating that the I4K2 molecules in the self-assembled structure are more deformed than KI4K with a smaller hydrophobic surface, which leads to a weaker hydrophobic interaction when the tapes stack along the side-chain direction. The hydrophobic effect in different systems can be quantified by measuring water fluctuation around large surfaces.<sup>57,58</sup> However, in our case,

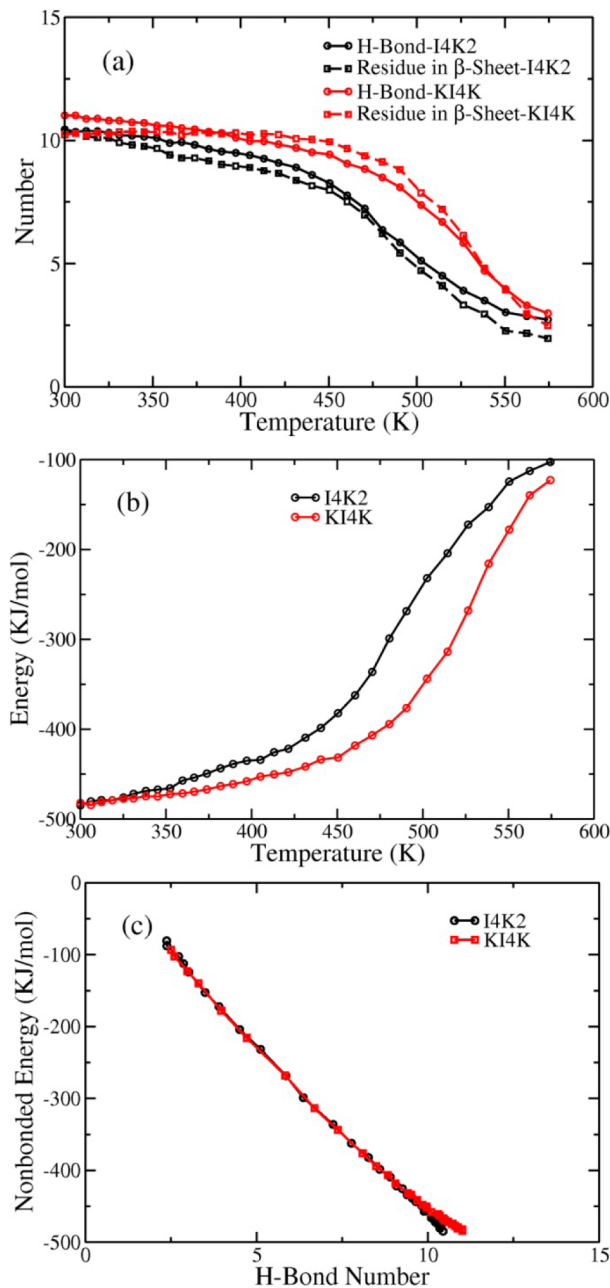


**Figure 6.** (a) Average numbers of hydrogen bonds and residues in  $\beta$ -sheet at different temperatures. (b) Average short-range energies between two neighboring peptides at different temperatures. (c) Nonbonded energies versus number of hydrogen bonds at different temperatures.

the surfaces of trimers are too small to see the difference between I4K2 and KI4K by performing the same calculations, as illustrated by the hydrophobic surface distributions shown in Figures S5 and S6 of the Supporting Information. In addition, the RMSD distributions between different monomers in trimer are shown in Figure 8b. The peak value for I4K2 is around 0.25 and 0.15 nm for KI4K, indicating that the structural difference between peptides in the self-assembled structure of I4K2 is much larger than KI4K, consistent with the results of the end-to-end distances.

From the above results, we can see that the nonbonded interactions, including hydrogen-bonding, VDW, and electrostatic interactions, between two neighboring peptides can

extend the backbones, and I4K2 molecules have a stronger propensity to bend than KI4K. The monomer structures are determined by the competition between hydrogen-bonding, electrostatic, and hydrophobic interactions, as described below. Since I4K2 and KI4K molecules have the same hydrophobic components, they have almost no differences in hydrophobic interactions, and free monomers tend to bend to minimize the exposure of the hydrophobic side chains. However, the electrostatic interactions are different due to different arrangements of charged lysine residues. For I4K2, both lysine residues are at one end of the peptide, so the bending of the molecule has no effect on the electrostatic interaction between the two charged lysine residues and does not result in the competition between hydrophobic and electrostatic interactions. For KI4K, since the bending of the molecule shortens the distance between two positively charged lysine residues at both ends, and thus increases the electrostatic interactions, the molecules are more difficult to bend, which competes with the hydrophobic interactions. In addition to the hydrogen bonds formed between neighboring peptides that drive the monomers to become more extended, the electrostatic interaction between the charged residues at two ends of KI4K drive the KI4K monomers to become more extended. Consequently, the less extended I4K2 in trimer have less hydrophobic surface than KI4K, which leads to smaller hydrophobic interaction for I4K2 tapes to stack along the side-chain direction. According to Aggelis's hierarchical model, the smaller stacking interaction between I4K2 tapes result in a smaller width than KI4K, consistent with the experimental results.<sup>23</sup>

When peptide molecules form the  $\beta$ -sheet structure, the backbones of neighboring peptides usually form a twist angle due to the intrinsic chirality of the backbone.<sup>59</sup> According to the hierarchical model,<sup>13,25,26</sup> the twist angle has a direct relation with the mesoscopic self-assembled morphology. The distributions of the average twist angle between the neighboring molecules of I4K2 and KI4K calculated by eq 3 are shown in Figure 9, which demonstrates that the twist angle between I4K2 is larger than KI4K, indicating that the I4K2 trimer is more twisted than KI4K. As described in Aggelis's hierarchical model,<sup>13,25,26</sup> a larger twist angle retards the layer stacking by increasing the elastic deformation energy cost for the hydrophobic stacking of two layers. Therefore, the I4K2 self-assembled structure is narrower than KI4K, consistent with the experimental observation.<sup>23</sup>

#### IV. CONCLUSIONS

In this work, we have performed atomistic MD simulations for monomers and REMD simulations for trimers for two kinds of peptides, I4K2 and KI4K, which have the same hydrophobic core but different charge residue orders. Our simulation results show that both peptides have a strong propensity to form  $\beta$ -sheet structures at  $T = 300$  K, but different arrangements of the charged lysine residues in I4K2 and KI4K lead to different trimer  $\beta$ -sheet structures. I4K2 has a dominant preferred trimer structure, while the three preferred trimer structures of KI4K have closer appearance probabilities. By comparing the structures and short-range energies from both monomer and trimer simulations, we have confirmed that the nonbonded short-range interactions between two neighboring peptides are the driving force to form the  $\beta$ -sheet structure and that the hydrogen bonds between two molecules stabilize the  $\beta$ -sheet structure. In the self-assembly process, the competition between hydrogen-bonding, hydrophobic, and electrostatic

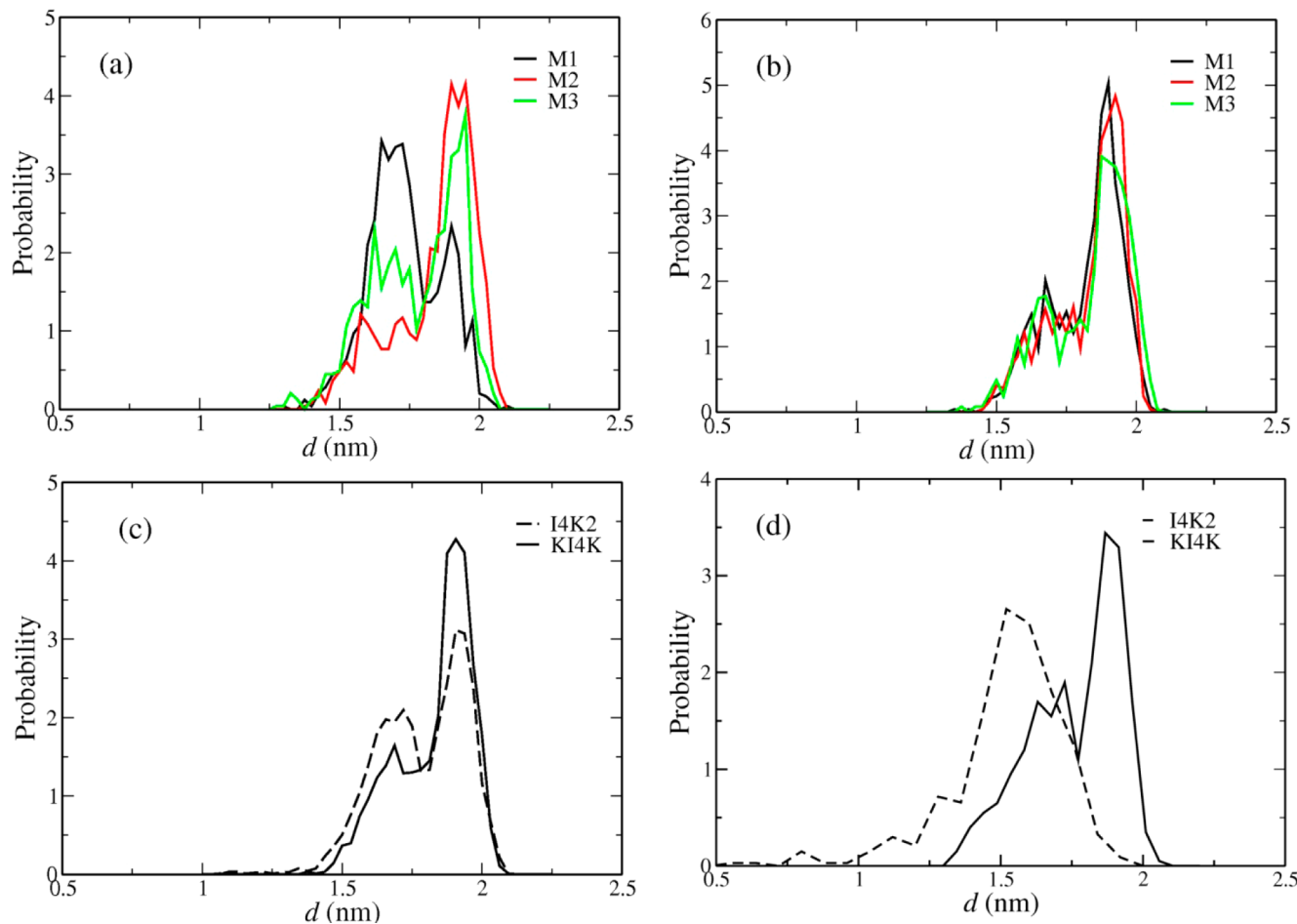


**Figure 7.** (a) End-to-end distances of the molecules in the I4K2 trimer. (b) End-to-end distances of the molecules in the KI4K trimer. (c) Average end-to-end distances in the REMD simulations. (d) End-to-end distances in the monomer MD simulations.

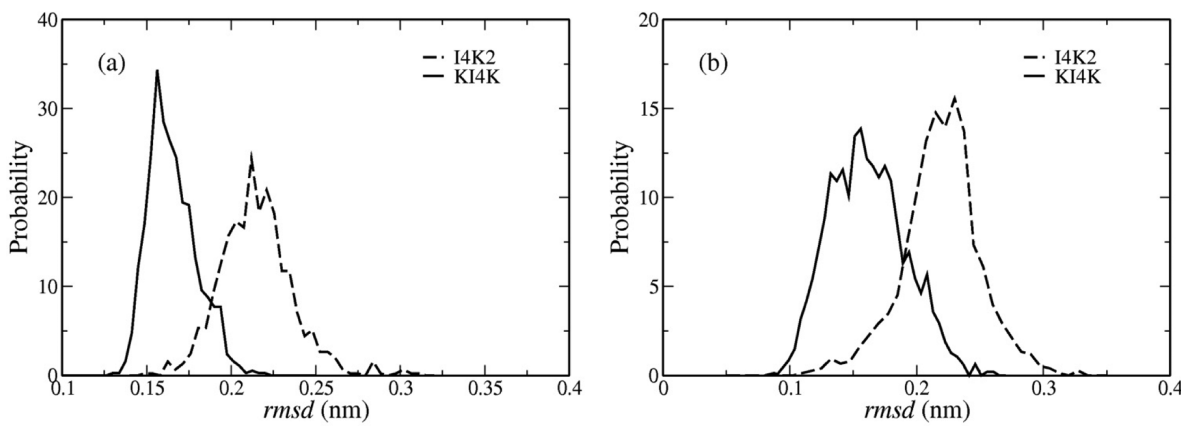


**Figure 8.** (a) RMSD between a peptide molecule in trimer and an ideally constructed fully extended peptide molecule. (b) RMSD between two peptide molecules in trimer.

interactions determines the stable trimer structures, which finally grow into the mesoscopic self-assembled structure. The hydrogen bonds between backbones tend to extend the monomer conformation for both I4K2 and KI4K. The intermolecular hydrophobic interactions force the molecules to aggregate, but the intramolecular hydrophobic interactions tend to make the molecules more coiled and deformable. The different arrangements of the charged lysine residues affect not only the conformation of a free monomer in solvent but also

the conformation of a monomer in trimer. The competition between repulsion from the two positively charged ends and effective hydrophobic interactions make it easier for KI4K to form an extended conformation than I4K2 and to have more hydrophobic surface exposed to the solvent. Therefore, KI4K has a stronger propensity to stack along the side-chain direction than I4K2. Moreover, the twist angle between neighboring molecules in I4K2 is also larger than in KI4K. According to Aggeli et al.'s model,<sup>13,25,26</sup> larger interlayer hydrophobic

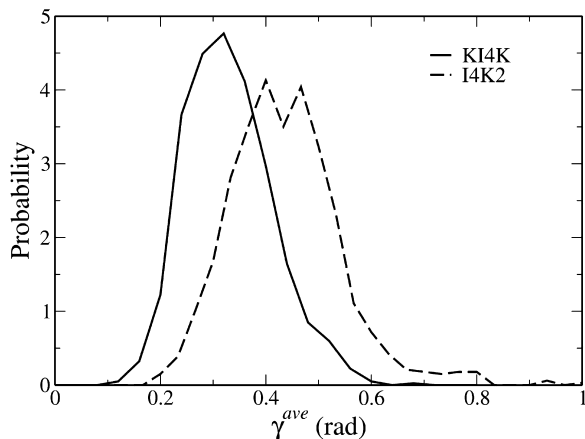


**Figure 9.** Distributions of the average twist angle between two neighboring peptides.

interactions lead to more layer stacking, while a larger twist angle reduces the layer stacking, so the KI4K self-assembled morphology can be wider than I4K2. Our simulation results and data analysis explain well the microscopic trimer structural differences of I4K2 and KI4K formed in the initial step of self-assembly, which finally lead to different mesoscopic self-assembled morphologies. This work not only provides a detailed microscopic mechanism for understanding the sensitivity of mesoscopic self-assembled morphologies to the subtlety of microscopic molecular structures but also serves as the basis for developing a systematic computational method for the prediction of peptide self-assembly.

## ■ ASSOCIATED CONTENT

### Supporting Information

Cryo-TEM images of I4K2 and KI4K self-assemblies and corresponding experimental details; center-of-mass distances between neighboring peptides; PMFs and hydrophobic surface distributions. This material is available free of charge via the Internet at <http://pubs.acs.org>.

## ■ AUTHOR INFORMATION

### Corresponding Authors

\*E-mail: wangyt@itp.ac.cn; Ph +86 10-62648749 (Y.W.).

\*E-mail: xuh@upc.edu.cn; Ph +86 532-86981569 (H.X.).

### Notes

The authors declare no competing financial interest.

## ■ ACKNOWLEDGMENTS

This work was supported by the National Natural Science Foundation of China (Nos. 91227115, 11121403, and 21033005) and the Scientific Research Foundation of China University of Petroleum (East China) for Young Scholar (Y1304073). H. Xu acknowledges support by the Program for New Century Excellent Talents in University (Grant NCET-11-0735). The authors thank Prof. Guanghong Wei for her helpful discussion. Prof. Robert K. Thomas's help with writing the manuscript is greatly appreciated. The authors also thank the Supercomputing Center in the Computer Network Information Center at the Chinese Academy of Sciences for allocations of computer time.

## ■ REFERENCES

- (1) Ulijn, R. V.; Smith, A. M. Designing Peptide Based Nanomaterials. *Chem. Soc. Rev.* **2008**, *37*, 664–675.
- (2) Whitesides, G. M.; Boncheva, M. Beyond Molecules: Self-Assembly of Mesoscopic and Macroscopic Components. *Proc. Natl. Acad. Sci. U. S. A.* **2002**, *99*, 4769–4774.
- (3) Whitesides, G. M.; Grzybowski, B. Self-Assembly at All Scales. *Science* **2002**, *295*, 2418–2421.
- (4) Yan, X. H.; Zhu, P. L.; Li, J. B. Self-Assembly and Application of Diphenylalanine-Based Nanostructures. *Chem. Soc. Rev.* **2010**, *39*, 1877–1890.
- (5) Zhang, S. G. Fabrication of Novel Biomaterials through Molecular Self-Assembly. *Nat. Biotechnol.* **2003**, *21*, 1171–1178.
- (6) Hilbich, C.; Kisters-Woike, B.; Reed, J.; Masters, C. L.; Beyreuther, K. Aggregation and Secondary Structure of Synthetic Amyloid  $\beta$ A4 Peptides of Alzheimer's Disease. *J. Mol. Biol.* **1991**, *218*, 149–163.
- (7) Barrow, C. J.; Yasuda, A.; Kenny, P.; Zagorski, M. G. Solution Conformations and Aggregational Properties of Synthetic Amyloid Beta-Peptides of Alzheimer's Disease: Analysis of Circular Dichroism Spectra. *J. Mol. Biol.* **1992**, *225*, 1075–1093.
- (8) Chiti, F.; Dobson, C. M. Protein Misfolding, Functional Amyloid, and Human Disease. *Annu. Rev. Biochem.* **2006**, *75*, 333–366.
- (9) Ross, C. A.; Poirier, M. A. Protein Aggregation and Neurodegenerative Disease. *Nat. Med.* **2004**, *10*, S10–S17.
- (10) Iwata, K.; Fujiwara, T.; Matsuki, Y.; Akutsu, H.; Takahashi, S.; Naiki, H.; Goto, Y. 3D Structure of Amyloid Protofilaments of Beta(2)-Microglobulin Fragment Probed by Solid-State NMR. *Proc. Natl. Acad. Sci. U. S. A.* **2006**, *103*, 18119–18124.
- (11) Jimenez, J. P.; Naki Guijarro, J.; Orlova, E.; Zurdo, J.; Dobson, M.; Sunde, M.; Saibil, H. Cryo-Electron Microscopy Structure of an SH3 Amyloid Fibril and Model of the Molecular Packing. *EMBO J.* **1999**, *18*, 815–821.
- (12) Sunde, M.; Serpell, L.; Bartlam, M.; Fraser, P.; Pepys, M.; Blake, C. Common Core Structure of Amyloid Fibrils by Synchrotron X-Ray Diffraction. *J. Mol. Biol.* **1997**, *273*, 729–739.
- (13) Aggeli, A.; Nyrkova, I. A.; Bell, M.; Harding, R.; Carrick, L.; McLeish, T. C. B.; Semenov, A. N.; Boden, N. Hierarchical Self-Assembly of Chiral Rod-Like Molecules as a Model for Peptide Beta-Sheet Tapes, Ribbons, Fibrils, and Fibers. *Proc. Natl. Acad. Sci. U. S. A.* **2001**, *98*, 11857–11862.
- (14) Reches, M.; Gazit, E. Formation of Closed-Cage Nanostructures by Self-Assembly of Aromatic Dipeptides. *Nano Lett.* **2004**, *4*, 581–585.
- (15) Baumann, M. K.; Textor, M.; Reinhult, E. Understanding Self-Assembled Amphiphilic Peptide Supramolecular Structures from Primary Structure Helix Propensity. *Langmuir* **2008**, *24*, 7645–7647.
- (16) Cui, H.; Muraoka, T.; Cheetham, A. G.; Stupp, S. I. Self-Assembly of Giant Peptide Nanobelts. *Nano Lett.* **2009**, *9*, 945–951.
- (17) Han, S. Y.; Cao, S. S.; Wang, Y. M.; Wang, J. Q.; Xia, D. H.; Xu, H.; Zhao, X. B.; Lu, J. R. Self-Assembly of Short Peptide Amphiphiles: The Cooperative Effect of Hydrophobic Interaction and Hydrogen Bonding. *Chem.—Eur. J.* **2011**, *17*, 13095–13102.
- (18) Hauser, C. A. E.; Deng, R. S.; Mishra, A.; Loo, Y. H.; Khoe, U.; Zhuang, F. R.; Cheong, D. W.; Accardo, A.; Sullivan, M. B.; Riekel, C.; et al. Natural Tri- to Hexapeptides Self-Assemble in Water to Amyloid Beta-Type Fiber Aggregates by Unexpected Alpha-Helical Intermediate Structures. *Proc. Natl. Acad. Sci. U. S. A.* **2011**, *108*, 1361–1366.
- (19) Tao, K.; Wang, J. Q.; Zhou, P.; Wang, C. D.; Xu, H.; Zhao, X. B.; Lu, J. R. Self-Assembly of Short a Beta(16–22) Peptides: Effect of Terminal Capping and the Role of Electrostatic Interaction. *Langmuir* **2011**, *27*, 2723–2730.
- (20) Yan, X. H.; Cui, Y.; He, Q.; Wang, K. W.; Li, J. B.; Mu, W. H.; Wang, B. L.; Ou-yang, Z. C. Reversible Transitions between Peptide Nanotubes and Vesicle-Like Structures Including Theoretical Modeling Studies. *Chem.—Eur. J.* **2008**, *14*, 5974–5980.
- (21) Lu, K.; Jacob, J.; Thiagarajan, P.; Conticello, V. P.; Lynn, D. G. Exploiting Amyloid Fibril Lamination for Nanotube Self-Assembly. *J. Am. Chem. Soc.* **2003**, *125*, 6391–6393.

- (22) Tjernberg, L.; Hosia, W.; Bark, N.; Thyberg, J.; Johansson, J. Charge Attraction and Beta Propensity Are Necessary for Amyloid Fibril Formation from Tetrapeptides. *J. Biol. Chem.* **2002**, *277*, 43243–43246.
- (23) Zhao, Y. R.; Wang, J. Q.; Deng, L.; Zhou, P.; Wang, S. J.; Wang, Y. T.; Xu, H.; Lu, J. R. Tuning the Self-Assembly of Short Peptides Via Sequence Variations. *Langmuir* **2013**, *29*, 13457–13464.
- (24) Frauenfelder, H.; Wolynes, P. G. Biomolecules: Where the Physics of Complexity and Simplicity Meet. *Phys. Today* **1994**, *47*, 58–64.
- (25) Nyrkova, I.; Semenov, A. N.; Aggeli, A.; Bell, M.; Boden, N.; McLeish, T. C. Self-Assembly and Structure Transformations in Living Polymers Forming Fibrils. *Eur. Phys. J. B* **2000**, *17*, 499–513.
- (26) Nyrkova, I.; Semenov, A. N.; Aggeli, A.; Boden, N. Fibril Stability in Solutions of Twisted-Sheet Peptides: A New Kind of Micellization in Chiral Systems. *Eur. Phys. J. B* **2000**, *17*, 481–497.
- (27) Armon, S.; Efrati, E.; Kupferman, R.; Sharon, E. Geometry and Mechanics in the Opening of Chiral Seed Pods. *Science* **2011**, *333*, 1726–1730.
- (28) Ghafouri, R.; Bruinsma, R. Helicoid to Spiral Ribbon Transition. *Phys. Rev. Lett.* **2005**, *94*, 138101.
- (29) Selinger, R. L. B.; Selinger, J. V.; Malanoski, A. P.; Schnur, J. M. Shape Selection in Chiral Self-Assembly. *Phys. Rev. Lett.* **2004**, *93*, 158103.
- (30) Ziserman, L.; Mor, A.; Harries, D.; Danino, D. Curvature Instability in a Chiral Amphiphile Self-Assembly. *Phys. Rev. Lett.* **2011**, *106*, 238105.
- (31) Childers, W. S.; Anthony, N. R.; Mehta, A. K.; Berland, K. M.; Lynn, D. G. Phase Networks of Cross-Beta Peptide Assemblies. *Langmuir* **2012**, *28*, 6386–6395.
- (32) Butterfoss, G. L.; Yoo, B.; Jaworski, J. N.; Chorny, I.; Dill, K. A.; Zuckermann, R. N.; Bonneau, R.; Kirshenbaum, K.; Voelz, V. A. De Novo Structure Prediction and Experimental Characterization of Folded Peptoid Oligomers. *Proc. Natl. Acad. Sci. U. S. A.* **2012**, *109*, 14320–14325.
- (33) Fishwick, C. W. G.; Beevers, A. J.; Carrick, L. M.; Whitehouse, C. D.; Aggeli, A.; Boden, N. Structures of Helical Beta-Tapes and Twisted Ribbons: The Role of Side-Chain Interactions on Twist and Bend Behavior. *Nano Lett.* **2003**, *3*, 1475–1479.
- (34) Garcia, A. E.; Sanbonmatsu, K. Y. Exploring the Energy Landscape of a Beta Hairpin in Explicit Solvent. *Proteins* **2001**, *42*, 345–354.
- (35) Karplus, M.; Kuriyan, J. Molecular Dynamics and Protein Function. *Proc. Natl. Acad. Sci. U. S. A.* **2005**, *102*, 6679–6685.
- (36) Wei, G. H.; Jewett, A. I.; Shea, J. E. Structural Diversity of Dimers of the Alzheimer Amyloid-Beta(25–35) Peptide and Polymorphism of the Resulting Fibrils. *Phys. Chem. Chem. Phys.* **2010**, *12*, 3622–3629.
- (37) Marini, D. M.; Hwang, W.; Lauffenburger, D. A.; Zhang, S. G.; Kamm, R. D. Left-Handed Helical Ribbon Intermediates in the Self-Assembly of a Beta-Sheet Peptide. *Nano Lett.* **2002**, *2*, 295–299.
- (38) Torrie, G. M.; Valleau, J. P. Nonphysical Sampling Distributions in Monte Carlo Free-Energy Estimation: Umbrella Sampling. *J. Comput. Phys.* **1977**, *23*, 187–199.
- (39) Kumar, S.; Rosenberg, J. M.; Bouzida, D.; Swendsen, R. H.; Kollman, P. A. The Weighted Histogram Analysis Method for Free-Energy Calculations on Biomolecules. I. The Method. *J. Comput. Phys.* **1992**, *13*, 1011–1021.
- (40) Hukushima, K.; Nemoto, K. Exchange Monte Carlo Method and Application to Spin Glass Simulations. *J. Phys. Soc. Jpn.* **1996**, *65*, 1604–1608.
- (41) Sugita, Y.; Okamoto, Y. Replica-Exchange Molecular Dynamics Method for Protein Folding. *Chem. Phys. Lett.* **1999**, *314*, 142–151.
- (42) Mondal, J.; Zhu, X.; Cui, Q. A.; Yethiraj, A. Self-Assembly of Beta-Peptides: Insight from the Pair and Many-Body Free Energy of Association. *J. Phys. Chem. C* **2010**, *114*, 13551–13556.
- (43) Mondal, J.; Yethiraj, A. Driving Force for the Association of Amphiphilic Molecules. *J. Phys. Chem. Lett.* **2011**, *2*, 2391–2395.
- (44) Gnanakaran, S.; Nussinov, R.; Garcia, A. E. Atomic-Level Description of Amyloid Beta-Dimer Formation. *J. Am. Chem. Soc.* **2006**, *128*, 2158–2159.
- (45) Bellesia, G.; Shea, J. E. What Determines the Structure and Stability of KFFE Monomers, Dimers, and Protofibrils? *Biophys. J.* **2009**, *96*, 875–886.
- (46) Van der Spoel, D.; Lindahl, E.; Hess, B.; Groenhof, G.; Mark, A. E.; Berendsen, H. J. C. Gromacs: Fast, Flexible, and Free. *J. Comput. Chem.* **2005**, *26*, 1701–1718.
- (47) Jorgensen, W. L.; Maxwell, D. S.; Titano-Rives, J. Development and Testing of the OPLS All-Atom Force Field on Conformational Energetics and Properties of Organic Liquids. *J. Am. Chem. Soc.* **1996**, *118*, 11225–11236.
- (48) Jorgensen, W. L.; William, L.; Chandrasekhar, J.; Madura, J. D.; Impey, R. W.; Klein, M. L. Comparison of Simple Potential Functions for Simulating Liquid Water. *J. Chem. Phys.* **1983**, *79*, 926–935.
- (49) Darden, T.; York, D.; Pedersen, L. Particle Mesh Ewald: An N-Log(N) Method for Ewald Sums in Large Systems. *J. Chem. Phys.* **1993**, *98*, 10089–10092.
- (50) Essmann, U.; Perera, L.; Berkowitz, M. L.; Darden, T.; Lee, H.; Pedersen, L. G. A Smooth Particle Mesh Ewald Method. *J. Chem. Phys.* **1995**, *103*, 8577–8593.
- (51) Nose, S. A Molecular Dynamics Method for Simulations in the Canonical Ensemble. *Mol. Phys.* **1984**, *52*, 255–268.
- (52) Hoover, W. G. Canonical Dynamics: Equilibrium Phase-Space Distributions. *Phys. Rev. A* **1985**, *31*, 1695–1697.
- (53) Parrinello, M.; Rahman, A. Polymorphic Transitions in Single Crystals: A New Molecular Dynamics Method. *J. Appl. Phys.* **1981**, *52*, 7182–7190.
- (54) Nose, S.; Klein, M. L. Constant Pressure Molecular Dynamics for Molecular Systems. *Mol. Phys.* **1983**, *50*, 1055–1076.
- (55) Daura, X.; Van Gunsteren, W.; Mark, A. Folding-Unfolding Thermodynamics of a  $\beta$ -Heptapeptide from Equilibrium Simulations. *Proteins: Struct., Funct., Genet.* **1999**, *34*, 269–280.
- (56) Kabasch, W.; Sander, C. Dictionary of Protein Secondary Structure: Pattern Recognition of Hydrogen-Bonded and Geometrical Features. *Biopolymers* **1983**, *22*, 2577–2637.
- (57) Patel, A. J.; Varilly, P.; Jamadagni, S. N.; Hagan, M. F.; Chandler, D.; Garde, S. Sitting at the Edge: How Biomolecules Use Hydrophobicity to Tune Their Interactions and Function. *J. Phys. Chem. B* **2012**, *116*, 2498–2503.
- (58) Patel, A. J.; Varilly, P.; Jamadagni, S. N.; Acharya, H.; Garde, S.; Chandler, D. Extended Surfaces Modulate Hydrophobic Interactions of Neighboring Solutes. *Proc. Natl. Acad. Sci. U. S. A.* **2011**, *108*, 17678–17683.
- (59) Weatherford, D. W.; Saleme, F. R. Conformations of Twisted Parallel Beta-Sheets and the Origin of Chirality in Protein Structures. *Proc. Natl. Acad. Sci. U. S. A.* **1979**, *76*, 19–23.